Catal Lett (2008) 122:121–130
DOI 10.1007/s10562-007-9357-5

Catalytic Performance of $Ce_{1-x}Ni_xO_2$ Catalysts for Propane Oxidative Steam Reforming

Lidia Pino · Antonio Vita · Francesco Cipitì · Massimo Laganà · Vincenzo Recupero

Received: 16 March 2007 / Accepted: 26 April 2007 / Published online: 4 December 2007

Abstract The catalytic activity of $Ce_{1-x}Ni_xO_2$ samples ($x = 0.05$; 0.10; 0.20) prepared by combustion synthesis have been evaluated in the Oxidative Steam Reforming of C_3H_8. The high activity and stability of $Ce_{0.95}Ni_{0.05}O_2$ and $Ce_{0.90}Ni_{0.10}O_2$ samples was ascribed to the co-existence of different Ni species: metallic, NiO highly dispersed and Ni^{2+} ions incorporated into CeO_2.

Keywords Propane oxidative steam reforming · Hydrogen production · Ceria-supported nickel catalysts

1 Introduction

Autothermal reforming (ATR) of hydrocarbons offers an advantageous route to produce H_2 for fuel cells systems. The process, combining steam reforming (SR) and catalytic partial oxidation (POX) reactions, to achieve an overall net heat balance, can be considered free from the disadvantages of the other methods, like slow start-up, considerable heat input or output, higher catalyst loadings, larger reactors and mass transfer limitations [1, 2]. Besides, temperature, pressure, O_2/fuel and H_2O/fuel ratios, can be selected as independent parameters to optimize the performance of the ATR process in terms of H_2 yield, to avoid coke deposition on catalyst or to minimize the by-products formation [3, 4].

Noble metal such as Pt, Rh, Ru [5, 6] have shown to be high active catalysts for the reforming reactions and excellent resistant to carbon formation but their low availability and high cost make them unsuitable for industrial size operations.

L. Pino (✉) · A. Vita · F. Cipitì · M. Laganà · V. Recupero
Institute CNR-ITAE, Via Salita S. Lucia sopra Contesse n. 5, S. Lucia, 98126 Messina, Italy
e-mail: lidia.pino@itae.cnr.it

Nickel has emerged as a possible alternative catalyst due to its low cost but tends to deactivate by coke formation. The use of CeO_2 as support or as additive in the traditional Ni/Al_2O_3 catalysts can contribute to enhance the catalytic activity and reduce the coke formation [7]; the important role of ceria played in catalytic reactions, is suggested to be the generation and participation of surface oxygen species and anionic vacancies [8, 9]. Recent studies have shown that these redox properties can be significantly enhanced if additional elements are introduced into lattice by forming a solid solution [10–12].

Previous investigations on Pt/CeO_2 catalysts have shown that strong metal-ceria interactions, by formation of solid solution in the mixed oxides catalysts, can be achieved by combustion synthesis of samples [13, 14]. The strong metal-to-support interaction appeared as one of the reasons of the observed high catalytic activity and stability during the hydrocarbons' partial oxidation and oxidative steam reforming (OSR).

In this paper, we report the performance allowed by $Ce_{1-x}Ni_xO_2$ catalysts, prepared by combustion synthesis, for the reaction of C_3H_8 with O_2 in presence of steam, referred as OSR. The structure and properties of the catalysts were investigated by X-Ray Diffraction (XRD), Temperature Programmed Reduction (TPR), X-Ray Photoelectron Spectroscopy (XPS) and Transmission Electron Microscopy (TEM).

2 Experimental

2.1 Catalysts Preparation

The $Ce_{1-x}Ni_xO_2$ ($x = 0.05$; 0.10; 0.20) catalysts were prepared by the combustion synthesis, the notation x in the

samples means the atomic ratio. Stoichiometric amounts of $(NH_4)_2Ce(NO_3)_6$, $Ni(NO_3)_2 \cdot 6H_2O$ and $C_2H_6N_4O_2$ (oxalyldihydrazide, as fuel) in aqueous solution were mixed in a borosilicate dish and heated at 350 °C to give a flaming combustion [15, 16]. The chemical reactions occurring in the combustion process can be written as follows:

$$5(NH_4)_2Ce(NO_3)_6 + 12C_2H_6N_4O_2 \rightarrow 5CeO_2 + 24CO_2 + 56H_2O + 44N_2. \quad (1)$$

$$Ni(NO_3)_2 + C_2H_6N_4O_2 \rightarrow NiO + 2CO_2 + 3H_2O + 3N_2. \quad (2)$$

$$5(1-x)\ (NH_4)_2Ce(NO_3)_6 + 5xNi(NO_3)_2 + 5C_2H_6N_4O_2 + 7(1-x)C_2H_6N_4O_2 \rightarrow 5Ce_{1-x}Ni_xO_2 + 10CO_2 + 14(1-x)CO_2 + 15H_2O + 41(1-x)H_2O + 15N_2 + 29(1-x)N_2 \quad (3)$$

$Ce_{0.95}Ni_{0.05}O_2$ sample was prepared by taking $(NH_4)_2Ce(NO_3)_6$, $Ni(NO_3)_2 \cdot 6H_2O$ and $C_2H_6N_4O_2$ in the molar ratio of 0.95:0.05:2.32. In a typical preparation 5 g of $(NH_4)_2Ce(NO_3)_6$, 0.138 g of $Ni(NO_3)_2 \cdot 6H_2O$ and 2.64 g of oxalyldihydrazide, dissolved in a minimum amount of water, were taken in a borosilicate dish and heated at 350 °C. After water evaporation, the mixture ignited with a cold flame leaving a sponge-like solid. Similary, samples with 0.10 and 0.20 atom% of Ni were also prepared. The catalysts, pellettized, calcined in air at 800 °C, crushed and sieved to 200–600 μm was tested without pre-reduction [15].

2.2 Catalysts Characterization

Powder XRD patterns were done with a Philips X-Pert 3710 diffractometer, using CuKα radiation at 40 kV and 20 mA. Continuous scans were collected with scan rates of 0.6°/min in the 2θ ranges 25°–80°. Peaks' positions, widths and lattice parameter were resolved by fitting profile using the Marquardt-Levenberg algorithm. The particle size of ceria and nickel phases was determined by Scherrer's equation, assuming a Gaussian shape of the peaks.

Temperature programmed reduction measurements were carried out by using 5% hydrogen in an argon mixture (30°cm^3/min, STP), as reducing gas, in a TPR reactor. The investigated temperature range was 0–1,000 °C, with a heating rate of 20 °C/min; the sample weight was set to keep the Ni load costant (111.5–28.1 mg). Hydrogen consumption was monitored by a thermoconductivity detector (TCD) connected to a PC for data storage and processing. The TCD response was quantitatively calibrated by monitoring the reduction of know amount of CuO, according to the procedure elsewhere described [17].

X-ray photoelectron spectra of the sample powders were recorded on a PHI Spectrometer (model 5800-01) equipped with an electron flood gun neutralizer and a monochromatic AlKα-source operating at 350 W. The X-ray photoelectron spectra were obtained with constant pass energy of 11.75 eV. Before spectral acquisition, samples were out-gassed overnight in the preparation chamber of the spectrometer. The characteristic photoemission peaks from Ce(3d), Ni(2p), O(1s) and C(1s) core levels were recorded for each sample. Binding energy were referenced to C1s of adventitious carbon at 284.6 eV. Peak fitting involved a deconvolution with the use of mixed Gaussian-Lorentzian functions. Both peak fitting and chemical analysis, as chemical composition, were carried out by using the PHI Multipak v.6 software.

Elemental analysis to detect the carbon deposition on the worked catalysts was carried out with a Carlo Erba CHNS analyzer (mod. EA 1108).

A Philips-CM12 transmission electron microscope (TEM), operated at 200 kV, was used for catalyst examination. Catalyst powder in isopropyl alcohol was supported on a holey 400 mesh copper grid.

2.3 Catalytic Activity Measurements

Catalytic activity tests on the OSR of C_3H_8 were conducted in a fixed-bed quartz reactor with inner diameter of 6 mm at atmospheric pressure. The catalyst sample was placed between two quartz wool plugs in the centre of a quartz tube, inserted into a furnace heated to the reaction temperature and controlled through a temperature controller. The reaction temperature was measured and controlled by two chromel-alumel thermocouples. One of the thermocouples was inserted into a thermowell and centred within the catalyst bed, while the other one was kept just at the outlet of the catalytic bed. The activity tests were carried out at 650 °C with gas hourly space velocity (GHSV, defined as volume per h of the gaseous feed at 0 °C and 1 bar of pressure per volume of the catalytic bed) of 5,000 h^{-1}. The feed and reaction products were analysed using an Agilent 6890 Plus gas chromatograph equipped with thermal conductivity and flame ionization detectors (FID). The CH_4, revealed to the TCD detector, was used as reference compound in FID analyses. The catalytic tests were initiated by heating the reactor, from ambient temperature to the 650 °C, under N_2 flow. Subsequently, N_2 flow was stopped and the reaction mixture (C_3H_8, O_2, steam, N_2) was allowed to flow through the reactor; a rapid temperature increase that stabilizes within some minutes to the set up value (650 °C) was observed.

On-line chromatographic analysis of the reaction products was carried out every 20 min during each test; the typical duration of each catalytic test was 6 h.

The reactants' conversion and products' selectivity were calculated according to the following equations:

$$S_{\text{carbon-containing product}} = \frac{F_{\text{carbon-containing product}}}{(F_{C_3H_8\text{in}} - F_{C_3H_8\text{out}}) \cdot n},$$

where $F_{\text{i, in or out}}$ was the molar flow rate of species i measured at inlet or at outlet of the reactor and n was the stoichiometric factor between the carbon-containing products and the C_3H_8. The Nitrogen peak was used for calibration of mass balance.

3 Results and Discussion

3.1 Structure of the Catalysts

Figure 1 shows the XRD patterns of the $Ce_{1-x}Ni_xO_2$ ($x = 0.05; 0.10; 0.20$) mixed oxides. For the $Ce_{0.95}Ni_{0.05}O_2$ sample the only presence of crystalline ceria with fluorite structure can be clearly observed, suggesting the presence of Ni as amorphous or highly dispersed and not revelable by diffraction. Weak diffraction peaks of metallic nickel, with such peaks intensity that increase with the Ni load, were detected for the remaining samples ($x = 0.10$ and 0.20); whereas, a scarcely visible broadening, due to the NiO phase can be envisaged with the sample at higher nickel content ($Ce_{0.80}Ni_{0.20}O_2$).

A careful examination of the patterns shows that the addition of nickel in the samples, determines a shift in the CeO_2 reflections to higher degree, as summarized in Table 1 for the three reticular planes (111), (200) and (220), that corresponds to a decrease in the ceria lattice parameter (α) compared with pure Ceria cell (5.4113 Å). However, the $\Delta 2\theta$ shift and the negative expansion in the ceria cell, increases with the addition of Ni from 0.05 to 0.10, whereas, intermediate values can be derived for the $Ce_{0.80}Ni_{0.20}O_2$ sample. These evidences can be related to the formation of an oxide solid solution in agreement with the observations previous reported by Lamonier et al. [18, 19].

The existence of a solid solution by replacement of Ce^{4+} with Ni^{2+} in the ceria lattice, can determine the shrinkage of the lattice which accounts for the evidence that the cation radius of Ni^{2+} (0.83 Å) are lower than that of Ce^{4+} (0.97 Å). The observed evolution of the shift in the ceria based samples indicates that the substitution of Ce^{4+} by Ni^{2+} increases up to 10at% of Ni, for higher amount (20at%) the solid solution decreases, in agreement with the observed segregation of NiO phase.

Finally, the CeO_2 particle size, derived by application of the Scherrer equation, ranges between 192 and 197 Å appearing as scarcely dependent from the nickel load; whereas the Ni particle size, undetected for the sample at lower metal content, increases from 174 to 209 Å with increasing the metal from 0.10 to 0.20 at%, as reported in Table 1. No quantification can be derived for the NiO phase.

In Fig. 2 the TPR profile of bulk NiO and $Ce_{1-x}Ni_xO_2$ samples are depicted. Pure NiO shows a sharp reduction peak (β) at about 420 °C followed by a small hump (γ) due to the big crystalline size, that retard the diffusion so its reduction proceeding as: $NiO \rightarrow Ni^{\delta+} \rightarrow Ni^{\circ}$, where β and γ

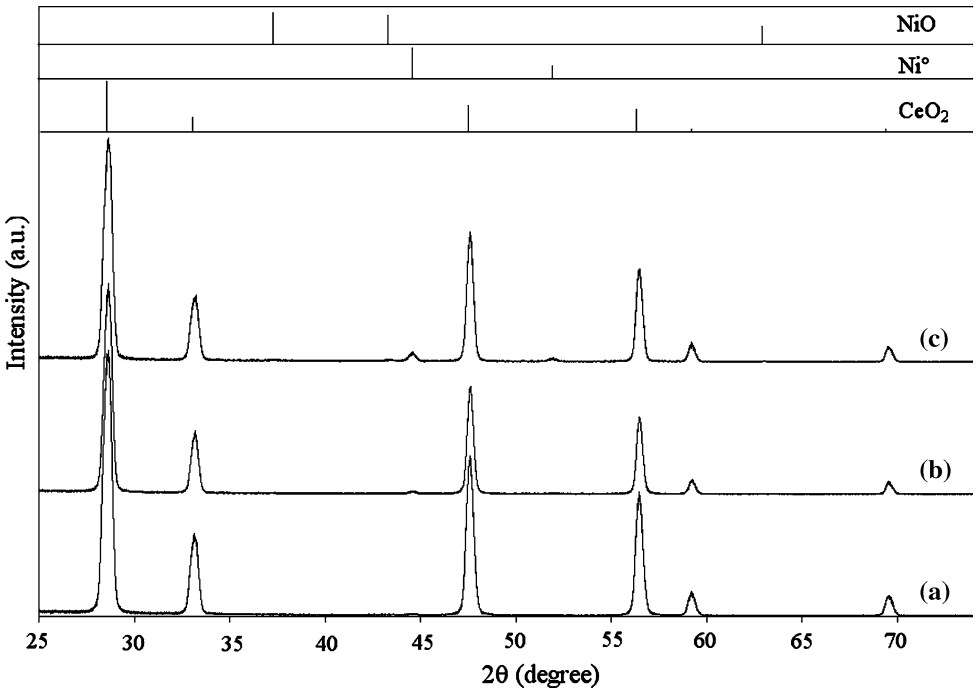

Fig. 1 XRD patterns of $Ce_{1-x}Ni_xO_2$ samples. **a** $Ce_{0.95}Ni_{0.05}O_2$; **b** $Ce_{0.90}Ni_{0.10}O_2$; **c** $Ce_{0.80}Ni_{0.20}O_2$ compared with the peaks position of the reference phases CeO_2 (JCPDS 4-594), NiO (JCPDS 4-835) and Ni (JCPDS 4-850)

Table 1 Physical properties of $Ce_{1-x}Ni_xO_2$ catalysts

Sample	Particle size (Å)[a]		CeO_2 Lattice parameter α (Å)[b]	CeO_2 $\Delta 2\theta$ shift (degree)[c]		
	CeO_2	Ni		(111)	(200)	(220)
$Ce_{0.95}Ni_{0.05}O_2$	194	–	5.3992	0.063	0.083	0.116
$Ce_{0.90}Ni_{0.10}O_2$	192	174	5.3936	0.093	0.108	0.135
$Ce_{0.80}Ni_{0.20}O_2$	197	209	5.3959	0.081	0.092	0.136

[a] Determined from CeO_2 and Ni (111) reflections according to the Scherrer equation

[b] Calculated from ceria (111) reflection from the equation $\alpha = \sqrt{h^2 + k^2 + l^2}(\lambda/2\sin\theta)$

[c] Measured by comparison with JCPDS files for the (111), (200) and (220) reticular planes ($\Delta 2\theta$ = peak position of the CeO_2 like phase in the mixed oxide – peak position of the reference CeO_2)

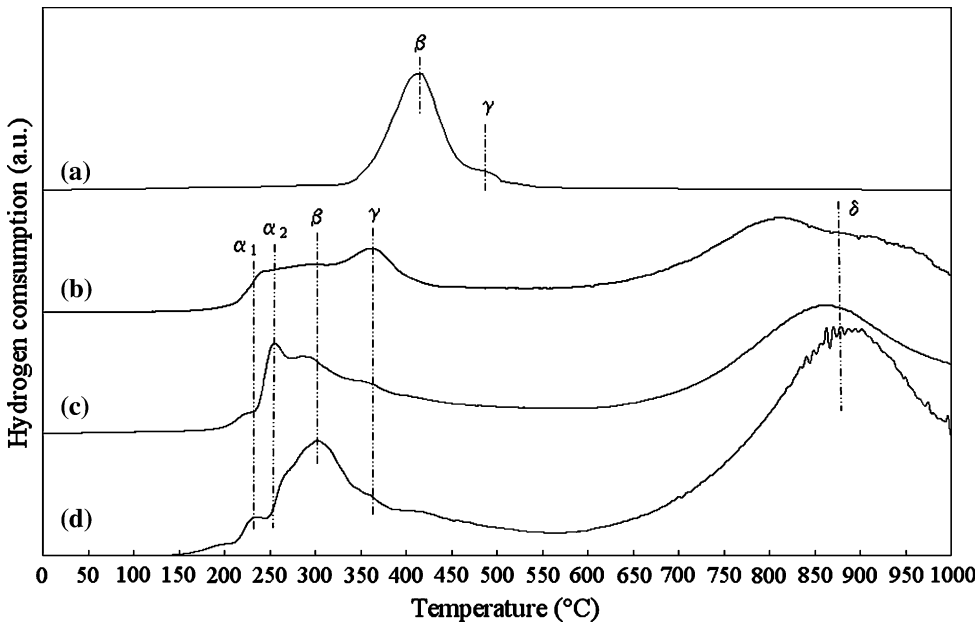

Fig. 2 TPR profile of NiO and $Ce_{1-x}Ni_xO_2$ catalysts. **a** NiO; **b** $Ce_{0.80}Ni_{0.20}O_2$; **c** $Ce_{0.90}Ni_{0.10}O_2$; **d** $Ce_{0.95}Ni_{0.05}O_2$

peaks represent the first and the second reduction step, respectively. For $Ce_{1-x}Ni_xO_2$ catalysts the β and γ peaks where shifted to lower temperature with the occurrence of new signals (α_1 and α_2) located at the temperatures' range included between 150 and 270 °C; whereas, the last signal (δ) observed at higher temperature (>650 °C) corresponds to the reduction of bulk ceria. The observed rearrangement of low temperature region suggests that are a lot of NiO_x sites which are strongly interacted with ceria, but different in the degree of this interaction.

The α_1 and α_2 peaks can be due to the reduction of adsorbed oxygen species; it was generally accepted that, the formation of solid solution by the incorporation of Ni^{2+} ions into the ceria lattice would results in the generation of oxygen vacancies, leading to the formation of active oxygen species, easy reducible by H_2 at low temperature [20]. Besides the β peak was generally assigned to the reduction of relatively free NiO that weakly interacts with surface of CeO_2 whereas, the γ peak is attributable to complex NiO strongly interacting with ceria.

XRD analysis showed the presence of Ni as solid solution in all the prepared samples, that results consistent with the occurrence of α_1 and α_2 reduction peaks. While, the absence of any reflection due to NiO in the sample at low metal amount ($x = 0.05$, 0.10) suggests that the particles can be very small or amorphous and nevertheless the reduction process was completed in two steps, as derived from the occurrence of β and γ peaks. This behaviour can suggests the presence of another NiO phase, probably NiO dispersed on CeO_2 or as solid solution more difficult to reduce. A quantitative estimation of the reduction peaks reveals that the H_2 uptake, exceeding that required for the NiO reduction in the $Ce_{0.95}Ni_{0.05}O_2$ sample, decreases with increasing the Ni content, as reported in Table 2.

This observation indicates that most of the H_2 consumed in the low temperature region can be associated to the removal of the readily available surface oxygen adjacent to the metal through a spillover mechanism. Increasing the Ni load ($x = 0.10$; 0.20) the H_2 uptake in both β and γ peaks decreases, while γ peak result enhanced much more than β

Table 2 Elemental analysis results and H_2 uptake (ml) during the TRP experiments of the $Ce_{1-x}Ni_xO_2$ catalysts

Sample	Bulk composition (wt%)[a]		H_2 uptake (ml)				H_2 (ml) needed to the NiO reduction[b]	Reduction degree of NiO (%)
	Ni	Ce	α_1	α_2	β	γ		
$Ce_{0.95}Ni_{0.05}O_2$	1.67 (1.75)	79.20 (79.21)	0.09	0.09	0.36	0.31	0.71	>100
$Ce_{0.90}Ni_{0.10}O_2$	2.97 (3.58)	78.93 (76.90)	0.02	0.14	0.22	0.25	0.64	99.8
$Ce_{0.80}Ni_{0.20}O_2$	8.19 (7.53)	74.12 (71.93)	0.01	0.06	0.17	0.27	0.88	57.8

[a] Number in parentheses are the calculated values

[b] Calculated by assuming the total reduction of NiO to Ni°

peaks, this can suggest the occurrence of a more pronounced interaction Me-support or the growth of larger crystallites of NiO, as evidenced from XRD analysis. The derived reduction degree of NiO, decreases with the increase of the Ni content due to the strong interaction between Ce and Ni in solid solution formed in lower Ni content sample; whereas in the $Ce_{0.80}Ni_{0.20}O_2$ the occurrence of large NiO particles can be responsible of the observed low reduction degree of NiO, as reported in Table 2.

The present results indicate that three types of NiO phases can be envisaged, Ni^{2+} species diffuse into the fluorite lattice to form a solid solution with ceria, NiO phase highly dispersed on CeO_2 and crystallized nickel oxide.

The X-ray photoelectron spectra of ceria are rather complex due to the hybridization between the 4f levels and the O2p states. As widely reported in literature [21–23], both Ce $3d_{5/2}$ and Ce $3d_{3/2}$ levels present five component v_o, v, v', v'', v''' and u_o, u, u', u'', u''', respectively (see Fig. 3). Because the insertion of nickel in the ceria lattice can increase the formation of Ce^{3+} species, XPS spectra of the present catalysts were studied in order to estimate the contribution of Ce^{4+} and Ce^{3+}. Generally, the high binding energy peak u'' is the best distinguished characteristic peak to differentiate Ce^{4+} from Ce^{3+}; the higher v''' and u''' peaks are not observed for purely trivalent ionic cerium compound (i.e. Ce_2O_3) [24]. The progressive reduction of CeO_2 into Ce_2O_3 determines a decrease of v''' and u''' peaks and an increase in v' and u' peaks at expense of v'' and u''. Romeo et al. [25] found that no direct correlation between the decrease in v''' intensity and the increase of v' exists, which was explained by a hybridization effect in the different structures. The spectral features due to Ce^{3+} are not clearly visible in the complex spectral envelope of the 3d region, a fitting procedure with the different Ce^{4+} and Ce^{3+} states was applied to the current experimental spectrum. The position of the well-resolved u''' peak was first obtained and then fixed the other peaks position, according to as reported by Zhang et al. [26]. Since the features characteristic of the Ce^{3+} states derives from the contribution of u_o, v_o, v' and u', the following equation was used to estimate the cerium oxide stoichiometry:

$$Ce^{3+}, (\%) = \frac{u_o + v_o + v' + u'}{\sum (u + v)},$$

referred to all states [27]; using this method, the fitted peak areas in the XPS spectra are used to estimate the contribution of Ce^{4+} and Ce^{3+} in the $Ce_{1-x}Ni_xO_2$ catalysts. Experimental XPS spectra with the results of peak fitting are shown in Fig. 3. The observed Ce^{3+} amount is

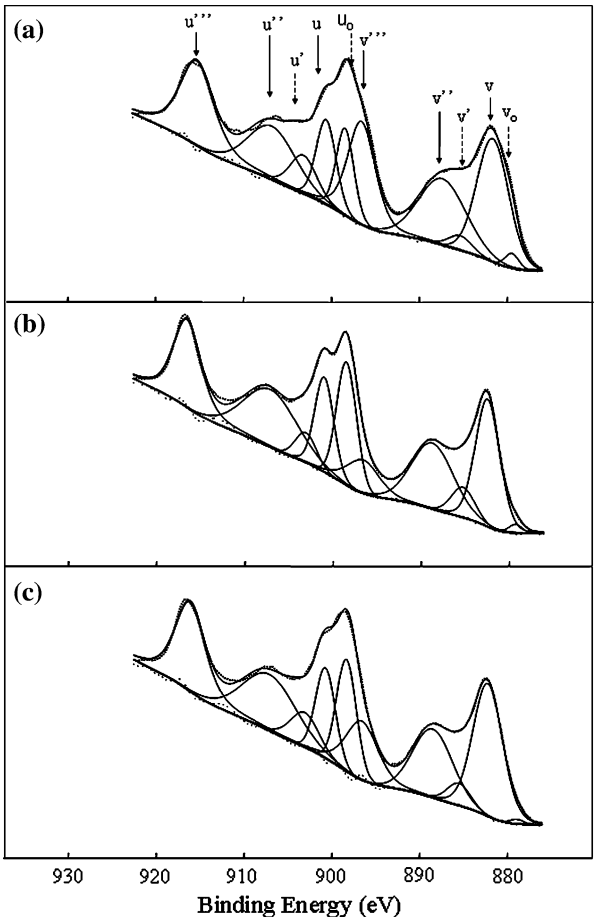

Fig. 3 Photoemission spectra of the Ce 3d region obtained from $Ce_{0.95}Ni_{0.05}O_2$ (**a**), $Ce_{0.90}Ni_{0.10}O_2$ (**b**) and $Ce_{0.80}Ni_{0.20}O_2$ (**c**) catalysts

Table 3 Binding energy (eV) of various species as obtained from Ni $2p_{3/2}$ X- ray photoelectron spectra, surface atomic ratios and Ce^{3+} concentration of $Ce_{1-x}Ni_xO_2$ catalysts

Sample	Ni/Ce^{a}_{bulk} (at%)	$Ni/Ce^{b}_{surface}$ (at%)	Ce^{3+} concentration (at%)	Species	Binding energy (eV)[c]
$Ce_{0.95}Ni_{0.05}O_2$	0.05	0.12	15.32	Ni^0	852.06 (14.1%)
				Ni^{2+}	854.12 (40.6%)
				Ni^{2+} satellite	859.59 (45.2%)
$Ce_{0.90}Ni_{0.10}O_2$	0.090	0.25	15.36	Ni^0	853.34 (15.7%)
				Ni^{2+}	855.51 (38.9%)
				Ni^{2+} satellite	860.80 (45.2%)
$Ce_{0.80}Ni_{0.20}O_2$	0.26	0.32	10.13	Ni^0	852.18 (2.97%)
				Ni^{2+}	854.74 (54.7%)
				Ni^{2+} satellite	860.47 (42.2%)

[a] Derived from X-ray fluorescence;

[b] From XPS data;

[c] Numbers in parentheses are the peak percentage

summarized in Table 3; a similar amount of Ce^{3+} species is observed with the increase of nickel load from 5 at% to 10 at%; further increase in the content of supported nickel (20 at%) induces a decrease of Ce^{3+} content. The incorporation of Ni in the CeO_2 lattice can lead to the reduction of some Ce^{4+} ions and to the creation of anionic vacancies [28, 29], yet this is particular observed for Ni content up to 10 at%; this evidence results consistent with previous observation derived from XRD analysis.

Figure 4 shows the XPS spectra in the Ni $2p_{3/2}$ region for the catalysts with different Ni content. The increase of intensity of the Ni 2p signals clearly appears with the increase of the Ni loading. As widely reported in literature [30], the most intense Ni $2p_{3/2}$ peak, located at about 854.0 eV, is characteristic of Ni $^{2+}$ ions in an oxygen environment. This peak is accompanied by a broader one due to shake-up processes, located at about 861.0 eV; this peak is the fingerprint of Ni^{2+} species and can be used to discriminate Ni^{2+} from Ni^{o} species. A careful study of the current spectra permits detecting a low-intensity shoulder at about 852.0 eV, which is characteristic of metallic nickel. To obtain a further information about the surface structure of the catalysts, the Ni $2p_{3/2}$ energy regions were fitted into three components: shake-up satellite line of unreduced Ni^{2+} ions at *ca*. 860 eV, Ni $2p_{3/2}$ principal peak of unreduced Ni^{2+} ions at about 854 eV and Ni $2p_{3/2}$ line of metallic nickel at *ca*. 852 eV. The results of peak fitting are summarized in Table 3. As clearly evidenced in Fig. 4 and Table 3, both Ni and NiO species were present in the samples. The binding energy associated with metallic nickel and Ni^{2+} species in the $Ce_{0.95}Ni_{0.05}O_2$ sample is significantly higher than the previously reported binding energy as related to unsupported species (Ni^{o}, 852 eV; NiO, 854 eV) [31]. Similar shift to larger energies was reported by Davison et al. [32] with 2.3 wt.% of NiO supported on ceria; it was suggested that this behaviour is due to an electronic interaction between nickel species and ceria, similar to the strong oxide-support interaction which has been proposed with PtO/CeO_2 materials [33].

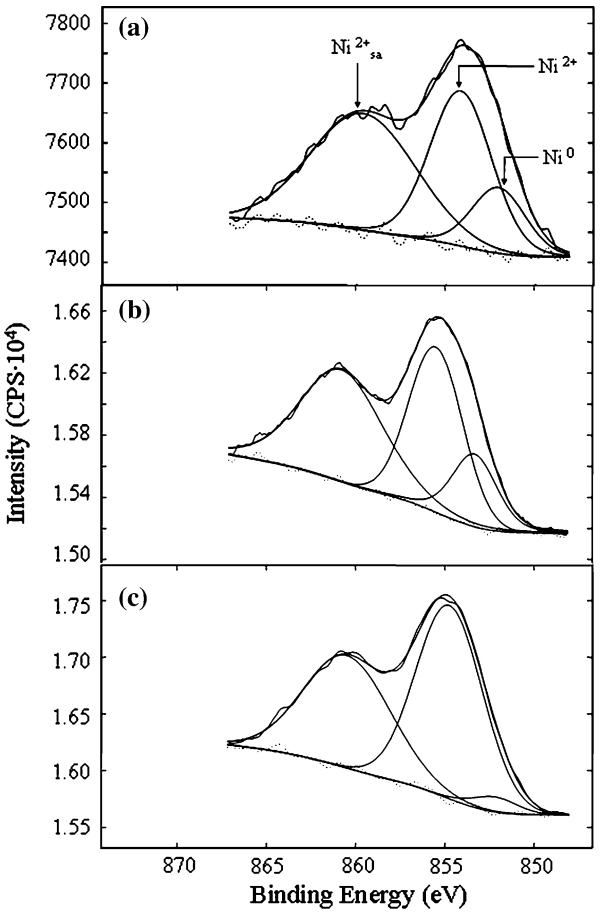

Fig. 4 Photoelectron spectra in the Ni $2p_{3/2}$ energy region of the ceria catalysts with different nickel loading : **a** $Ce_{0.95}Ni_{0.05}O_2$; **b** $Ce_{0.90}Ni_{0.10}O_2$; **c** $Ce_{0.80}Ni_{0.20}O_2$

Increasing the Nickel load (10at%) a more pronounced shift can be observed, while with the 20at% of Ni content both peaks result in intermediate position between the ones previously given for 5 and 10 at% Ni, respectively, in good accordance with XRD results.

3.2 Catalytic Activity

The stoichiometry of C_3H_8 ATR, where the combined heats of reaction of exothermic partial oxidation with air (POX) and endothermic steam reforming (SR) are balanced, can be schematized as:

$$C_3H_8 + \varepsilon(O_2 + 3.76\ N_2) + (6 - 2\varepsilon)H_2O \rightarrow 3CO_2 + (10 - 2\varepsilon)\ H_2 + 3.76\ \varepsilon\ N_2. \quad (4)$$
$$\Delta H_{298} = 152.59 - (136.64\varepsilon)\ \text{kcal mol}^{-1}$$

Exothermic total oxidation ($C_3H_8 + 5O_2 \rightarrow 3CO_2 + 4\ H_2O$) followed by steam ($C_3H_8 + 3H_2O \rightarrow 3CO + 7H_2$) and CO_2 reforming ($C_3H_8 + 3CO_2 \rightarrow 6CO + 4H_2$) reactions, followed by the establishment of water gas shift ($CO + H_2O \rightarrow CO_2 + H_2$) and methanation ($CO + 3\ H_2 \rightarrow CH_4 + H_2O$) equilibria, generally play a role that depends on reactants composition, temperature, gas hourly space velocity and catalytic system involved.

The catalytic activity of the current $Ce_{1-x}Ni_xO_2$ samples has been evaluated under an exothermic regime (O/C = 1.33, $\varepsilon = 2$; $\Delta H_{298} = -120.7$ kcal mol^{-1}), defined as OSR, by decreasing the excess of steam (in order to minimize the coke formation, S/C = 1.20) to the stoichiometric value (S/C = 0.66). However, the selected O/C ratio has been derived from preliminary partial oxidation experiments and in accordance with literature value [34, 35] that suggest an optimum O/C ratio of 1.25 to produce synthesis gas. Increasing the O/C ratio, the H_2 selectivity and propane conversion increase, while the associated total olefins' production decreases. The steam addition (S/C = 0.66–1.20) in the present OSR experiments determines a further increase in the O/C ratio (including O_2 and H_2O oxygen) ranging between 2.0 and 2.5, respectively that can contribute to minimize both by-products formation and carbon deposition.

Table 4 gives the detailed reaction results in OSR. Total O_2 and C_3H_8 conversion was observed with $Ce_{0.95}Ni_{0.05}O_2$ sample, H_2, CO, CO_2 and CH_4 are the main products. The H_2 concentration increases with the increase of the S/C, while the derived H_2/CO_x ratio, ranging between 1.4 and 1.5 results close to the partial oxidation value (H_2/CO = 1.3).

Concerning partial oxidation, a number of recent studies have indicated that the process is a combination of catalytic combustion where all the O_2 is consumed, followed by steam reforming of un-reacted propane [36, 38]. In accordance with this mechanism, with O/C = 1.33 a fraction (40%) of the fed C_3H_8 can be totally oxidized; secondly steam reforming of un-reacted propane with the produced steam and WGS reactions produces H_2, CO and CO_2. The remaining C_3H_8, not involved in the combustion reaction, in presence of the introduced steam can be involved at the same time in a secondary steam reforming reaction ($C_3H_8 + 6H_2O \rightarrow 3CO_2 + 10\ H_2$) which occurs in excess of steam. The produced CO_2 determines the high H_2/CO ratio observed; increasing the S/C ratio in the feed, the contribution of secondary steam and water gas shift reactions, increases, as revealed by the increase in H_2/CO ratio (from 3.28 to 4.0) and by the decrease in the CO selectivity. However, the CH_4 appearance in the system decreases with increasing the steam content; this evidence can be related to reforming of formed CH_4 to CO, CO_2 and H_2 by the excess of steam or to a decrease in the

Table 4 OSR activity of $Ce_{1-x}Ni_xO_2$ catalyst at 650 °C with GHSV = 5000 h^{-1} and O/C = 1.33

Sample	S/C	C_3H_8 conversion (%)	O_2 conversion (%)	H_2 concentration (%)[a]	H_2/CO	H_2/CO_x	Selectivity					
							CO (%)	CO_2 (%)	CH_4 (%)	C_2H_6 (%)	C_2H_4 (%)	C_3H_6 (%)
$Ce_{0.95}Ni_{0.05}O_2$	1.20	100	100	24.4 (25.0)	4.00	1.52	36.93	60.22	2.85	–	–	–
	1.00	100	100	24.4 (25.0)	3.70	1.44	37.65	59.15	3.20	–	–	–
	0.66	100	100	23.8 (24.8)	3.28	1.41	41.42	54.76	3.82	–	–	–
$Ce_{0.80}Ni_{0.20}O_2$	1.20	100	100	25.00	4.07	1.57	37.80	59.66	2.54	–	–	–
	1.00	100	100	25.00	3.60	1.52	41.20	56.00	2.80	–	–	–
	0.66	100	100	24.54	3.00	1.42	45.65	50.62	3.74	–	–	–
$Ce_{0.90}Ni_{0.10}O_2$	1.20	99.48	97.70	19.26	2.78	1.35	41.73	43.86	4.06	0.48	7.98	1.89
	1.00	99.44	97.35	19.16	2.42	1.26	44.54	40.88	4.41	0.47	7.86	1.85
	0.66	99.40	97.04	19.13	2.26	1.24	46.60	38.35	4.87	0.42	7.80	1.96

[a] Numbers in parenthesis are the thermodynamic predicted values

exothermicity of the reaction that can minimize the C_3H_8 thermal craking ($C_3H_8 \rightarrow C_2H_4 + CH_4$).

The present results can be related to the different features of the catalysts envisaged from the as reported characterizations: high dispersion of NiO on catalysts, undetected by XRD diffraction, presence of metallic Ni (from XPS and XRD investigations) and the high reduction degree of NiO, evidenced by TPR study.

Partial oxidation and steam reforming proceed via the dissociative adsorption of C_3H_8 and/or O_2 on metallic sites, whereas the support provides sites for water activation into hydroxyl group [39, 40]. NiO highly dispersed on the support and Ni^{2+} incorporated into the ceria lattice becomes additional sites for the adsorption of C_3H_8 and O_2, more favoured than H_2O adsorption. The surface defect of ceria, related to the presence of Ce^{3+}, are preferential sites for oxygen adsorption, as a consequence local reducing environment can be generated able to make the direct interaction of C_3H_8 with lattice oxygen over NiO, represented as:

$$C_3H_8 + 8Ni^{2+} + 8O^{2-} \rightarrow 2CO_2 + 4H_2O + 8Ni^0 + 8V^{\bullet\bullet}, \quad (5)$$

where, $V^{\bullet\bullet}$ denotes the oxygen anion vacancies.

Ni^{2+} incorporated into the ceria lattice to form a solid solution, makes CeO_2 form oxygen vacancies which can adsorb gas oxygen, enhancing the C_3H_8 combustion [20].

A light decrease in the catalyst performance, with the occurrence of by-products (C_2H_6, C_2H_4 and C_3H_6), was revealed with $Ce_{0.80}Ni_{0.20}O_2$ sample; a substantial lower H_2 content, related to the incomplete reagents' conversion was observed, along all the investigated S/C ratios. This evidence can be mainly ascribed to the lower presence of metallic nickel sites on the catalyst surface, as evidenced from XPS; while the presence of solid solution can promote the C_3H_8 total oxidation, in accordance with the derived H_2/CO and H_2/CO_x ratios.

Very exiguous carbon deposition can be derived with $Ce_{0.95}Ni_{0.05}O_2$ and $Ce_{0.90}Ni_{0.10}O_2$ samples at low S/C ratio in the feed, as emerged from CHNS elemental analysis on spent catalyst compared with the C amount derived by calculation of carbon balance and from the observed invariant pressure drop in the catalytic bed (reported in Table 5). Whereas, low carbon accumulation (0.154 mmol for gram of catalyst) was detected with $Ce_{0.80}Ni_{0.20}O_2$ sample that result consistent with the appearance of pressure drop and with the noticeable value (13.5 mmol/g catalyst) derived from the carbon balance.

Boudard reaction and decomposition of hydrocarbons are the main pathways for carbon deposition [41, 42], with the increase of the S/C ratio the equilibrium of water gas shift reaction moves forward and produces more CO_2 rather than CO, as evidenced in Table 4. In presence of solid solution on the catalytic system, the high mobility of lattice oxygen can contribute to the removal of carbon species on the surface by the gas-solid reaction between hydrocarbons with lattice oxygen, forming H_2 and CO_2. Parallel reactions of the support near the metal-oxide interface, where an oxygen deficient composition was expected, can favour CO_2 and H_2O conversion ($Ce_{2-x}O_2 + H_2O \rightarrow CeO_2 + H_2$; $Ce_{2-x}O_2 + CO_2 \rightarrow CeO_2 + CO$), according to [43, 44].

Table 5 Carbon deposition during the OSR with the $Ce_{1-x}Ni_xO_2$ catalysts (GHSV= 5000 h^{-1}, O/C = 1.33, S/C = 0.66)

Sample	ΔP (atm)[a]	C (mmoli/g catalyst)	C (mmoli/g catalyst)[b]
$Ce_{0.95}Ni_{0.05}O_2$	0	0.05	0.002
$Ce_{0.80}Ni_{0.20}O_2$	0	2.00	0.012
$Ce_{0.90}Ni_{0.10}O_2$	0.05	13.50	0.154

[a] Pressure drop measured along the catalytic bed

[b] From CHNS analysis

3.3 Stability Test of $Ce_{0.95}Ni_{0.05}O_2$ Sample

The stability of the catalysts was performed on $Ce_{0.95}Ni_{0.05}O_2$ sample at 650 °C, with O/C = 1.33 and S/C = 1.20 at a GHSV of 5,000 h^{-1}, as shown in Fig. 5. Aim of the test, carried out with sequential start-up and shut-down cycles after about 6 h of reaction, was to highlight the phenomena related to the catalyst decay, such as metal sintering and/or carbon deposition. Total propane and oxygen conversion was observed along the run with a constant H_2 concentration of about 25%, no visible deactivation of the catalysts was observed throughout the 100 h of reaction.

Transmission electron microscopy investigation, carried out on spent catalyst confirm, as shown in Fig. 6, the absence of carbon deposition.

The reported results suggest that excess steam in a traditional steam reforming process to avoid coke formation, can be replaced by oxygen over the proposed catalyst, reducing additional steam cost. Furthermore, OSR could be carried out in an adiabatic reactor without external heat supply, achieving the combination of exothermic partial oxidation and endothermic steam reforming.

The present findings may provide new opportunities for the rational design of new advanced mixed oxide catalyst systems for more efficient H_2 production. The combustion synthesis method suggests the possibility of producing in a single stage the oxide precursor of a supported catalyst. Key aspects, like the preparation of samples with reproducible phases' composition and catalytic properties, require further investigations.

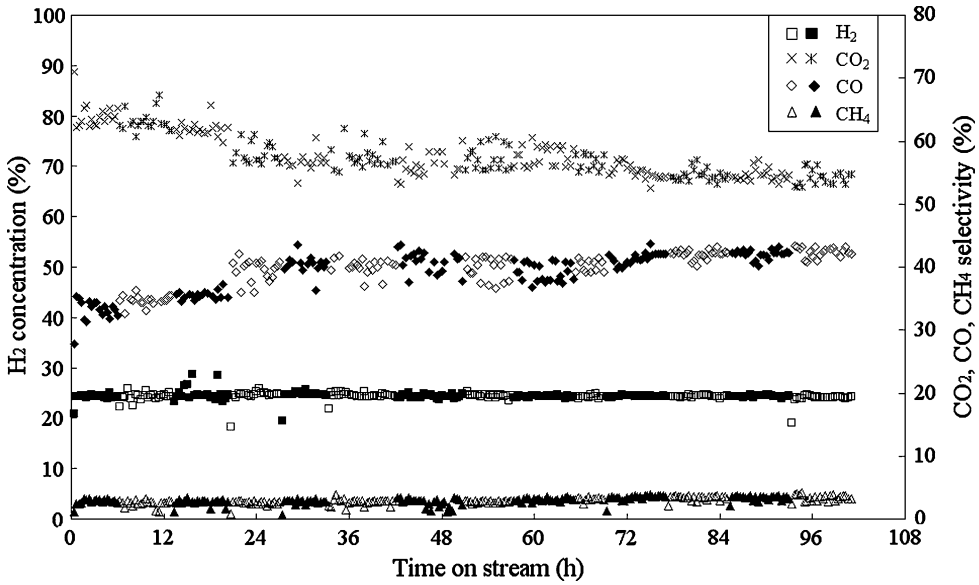

Fig. 5 Stability test performed on $Ce_{0.95}Ni_{0.05}O_2$ sample under sequential start-up and shut-down cycles at 650 °C with O/C = 1.33, S/C = 1.20 and GHSV = 5,000 h^{-1}

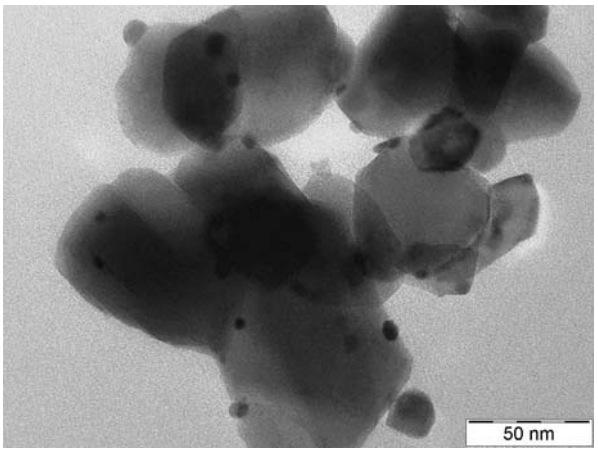

Fig. 6 TEM image of spent $Ce_{0.95}Ni_{0.05}O_2$ sample after the stability test

4 Conclusions

We describe the synthesis of $Ce_{1-x}Ni_xO_2$ ($x = 0.05$; 0.10; 0.20) catalyst by combustion method. These materials showed promising catalytic activity in the OSR to generate synthesis gas. Combined XRD, TPR, XPS demonstrate the co-existence of three kinds of Ni phase: metallic nickel, highly dispersed NiO on the surface of CeO_2 and Ni incorporated into the ceria lattice. $Ce_{0.95}Ni_{0.05}O_2$ sample showed good stability in absence of carbon deposition along 100 h of reaction.

References

1. Zalc JM, Löffler DG (2002) J Power Sources 11:58
2. Ayabe S, Omoto H, Utaka T, Kikuchi R, Sasaki K, Terooka Y, Eguchi K (2003) Appl Catal A 241:261
3. Ahmed S, Krumpelt M (2001) Int J Hydrogen Energy 26:291
4. Moon DJ, Steekumar K, Lee SD, Lee BG, Kim HS (2001) Appl Catal A 215:1
5. Krumpelt M, Krause TR, Carter JD, Kopasz JP Ahmed S (2002) Catal Today 77:3
6. Qi A, Wang S, Fu G, Wu D (2005) Appl Catal A 293:71
7. Wenying L, Jie F, Kechang X (1998) React Kinet Catal Lett 64:381
8. Laosiripojana N, Sutthisripok W, Assabunsrungrat S (2005) Chem Eng J 112:13
9. Laosiripojana N, Assabunsrungrat S (2006) J Power Sources 158:1348
10. Trovarelli A, de Leitenburg C, Dolcetti G (1997) Chemtech 27:32
11. Potdar HS, Roh H-S, Jun K–W, Ji M, Liu Z-W (2002) Catal Lett 84:95
12. Yisup N, Cao Y, Feng W-L, Dai W-L, Fan K–N (2005) Catal Lett 99:207
13. Pino L, Vita A, Cordaro M, Recupero V, Hegde MS (2003) Appl Catal A 243:135
14. Pino L, Vita A, Cipitì, Laganà M, Recupero V (2006) Appl Catal A 306:68
15. Patil KC, Aruna ST, Mimami T (2002) Curr Opin Solid State Mater Sci 6:507
16. Lian JS, Zhang XY, Zhang HP, Jiang ZH, Zhang J (2004) Mater Lett 58:1183
17. Spadaro L, Arena F, Granados ML, Ojeda M, Fierro JLG, Frusteri F (2005) J Catal 234:451
18. Lamonier C, Ponchel A, D'Huysser A, Jalowiecki-Duhamel L (1999) Catal Today 50:247
19. Ponchel A, Huysser AD, Lamonier C, Jalowiechi-Duhamel L (2000) Phys Chem Chem Phys 2:303
20. Shan W, Luo M, Ying P, Shen W, Li C (2003) Appl Catal A 246:1
21. Le Normand F, El Fallah J, Hilaire H, Legaré P, Kotani A, Parlebas C (1989) Solid State Comm 71:885
22. Pfau A, Scheierban KD (1994) Surf Sci 321:71–80
23. Le Normand F, Hilaire L, Kili K, Krill G, Maire G (1988) J Phys Chem 92:2561–2568
24. Mullins DR, Overbury SH, Hunsteey DR (1998) Surf Sci 409:307
25. Romeo M, Bark K, El Fallah J, Le Normand F, Hilaire L (1993) Surf Interface Anal 20:508–512

26. Zhang F, Wang P, Koberstein J, Khalid S, Chen S–W (2004) Surf Sci 563:74–82
27. El Fallah J, Hilaire L, Romeo M, Le Normand F (1995) J Electron Spectrosc Relat Phenom 73:89–103
28. Wrobel G, Sohier MP, D'Huysser A, Bonnelle JP, Marcq JP (1993) Appl Catal A 101:73
29. Wrobel G, Lamonier C, Bannani A, D'Huysser A, Aboukais A (1996) J Chem Soc Faraday Trans 92:2001
30. Carley AF, Jackson SD, O'Shea JN, Roberts MW (2001) Phys Chem Chem Phys 3:274
31. Espinós JP, Gonzáles-Elipe AR, Fernández A, Munera G (1992) Surf Interface Anal 19:508
32. Davidson A, Tempere JF, Che M, Roulet H, Dufour G (1996) J Phys Chem 100:4919–4929
33. Murrell LL, Tauser SJ, Anderson DR (1991) In: Crucq A (ed) Catalysis and automotive pollution control II. Elsevier, Amsterdam, p 275
34. Huff M, Schmidt LD (1994) J Catal 149:127
35. Silberova B, Venvik HJ, Holmen A (2005) Catal Today 99:69
36. Barbier J, Duprez D (1992) Appl Catal A 85:89
37. Weng WZ, Chen MS, Yan QG, Wu TH, Chao ZS, Liao YY, Wan HL (2000) Catal Today 63:317
38. Guerrero-Ruiz A, Ferreira-Aparicio P, Bachiller-Baeza MB, Rodriguez-Ramos I (1998) Catal Today 46:99
39. Duprez D, Miloudi A, Delahay G, Maurel R (1984) J Catal 90:292
40. Wang W, Gorte RJ (2002) Appl Catal A 224:209
41. Claridge JB, Green MLH, Tsang SC, York APE, Ashcroft AT, Battle PD (1993) Catal Lett 22:299
42. Laosiripojana N, Saugtonkitcharoen W, Assabumrungrat S (2006) Fuel 85:323
43. Otsuka K, Wang Y, Sunada E, Yamanaka I (1998) J Catal 175:152
44. Sharma S, Hilaire S, Vohs JM, Gorte RJ, Jen HW (2000) J Catal 190:199